Title: Understanding the impacts of Al^{+3}-substitutions on the enhancement of magnetic, dielectric and electrical behaviors of ceramic processed nickel-zinc mixed ferrites: FTIR assisted studies

Authors: Tapos Kumar Bromho, Khalil Ibrahim, Humayun Kabir, M. Mahbubur Rahman, Kamrul Hasan, Tahmina Ferdous, Hatem Taha, Mohammednoor Altarawneh, Zhong-Tao Jiang

PII: S0025-5408(17)31186-8
DOI: http://dx.doi.org/10.1016/j.materresbull.2017.09.013
Reference: MRB 9553

To appear in: *MRB*

Received date: 11-5-2017
Revised date: 16-7-2017
Accepted date: 8-9-2017

Please cite this article as: Tapos Kumar Bromho, Khalil Ibrahim, Humayun Kabir, M.Mahbubur Rahman, Kamrul Hasan, Tahmina Ferdous, Hatem Taha, Mohammednoor Altarawneh, Zhong-Tao Jiang, Understanding the impacts of Al+3-substitutions on the enhancement of magnetic, dielectric and electrical behaviors of ceramic processed nickel-zinc mixed ferrites: FTIR assisted studies, Materials Research Bulletinhttp://dx.doi.org/10.1016/j.materresbull.2017.09.013

Understanding the impacts of Al^{+3}-substitutions on the enhancement of magnetic, dielectric and electrical behaviors of ceramic processed nickel-zinc mixed ferrites: FTIR assisted studies

Tapos Kumar Bromho[1], Khalil Ibrahim[2,3], Humayun Kabir[4,5], M. Mahbubur Rahman[2,5*], Kamrul Hasan[6], Tahmina Ferdous[5], Hatem Taha[2,7], Mohammednoor Altarawneh[2], Zhong-Tao Jiang[2]

[1]Department of Chemistry & Physics, Gono University, Savar, Dhaka, Bangladesh
[2]Surface Analysis and Materials Engineering Research Group
School of Engineering & Information Technology, Murdoch University, Perth, Western Australia 6150, Australia
[3]Department of Mechanical Engineering, Karbala Institute of Technology, Karbala 51214, Iraq
[4]School of Metallurgy and Materials, University of Birmingham, Birmingham, United Kingdom
[5]Department of Physics, Jahangirnagar University, Savar, Dhaka 1342, Bangladesh
[6]Department of Chemistry, College of Sciences, University of Sharjah, P. O. Box 27272, Sharjah, United Arab Emirates
[7]College of Ibn-Alhaitham for Pure Science, University of Baghdad, Baghdad, Iraq

[*]Corresponding author's email: m.rahman@murdoch.edu.au

Graphical abstract

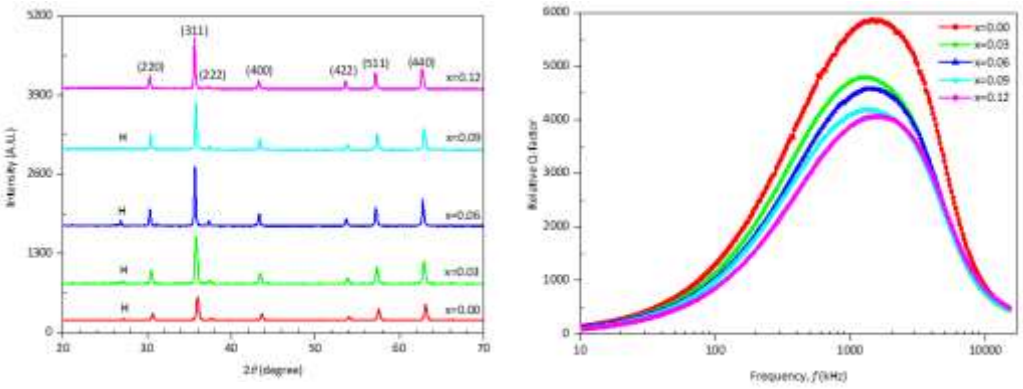

Highlights

1. Al-doped ceramic Ni-Zn ferrites are studied
2. Octahedral and tetrahedral vibrations were confirmed via FTIR studies
3. Curie temperature was systematically reduced with subsequent Al-doping
4. AC resistivity and loss tangent were significantly reduced with Al-content
5. Dielectric behaviour was associated with the bi-layer space-charge polarization

Abstract

Al-incorporated Ni-Zn ferrites ($Ni_{0.65}Zn_{0.35}Al_xFe_{2-x}O_4$, where x = 0, 0.03, 0.06, 0.09, 0.12) synthesized *via* standard ceramic technology were investigated for their structural, magnetic, dielectric, and electrical properties. Al substitution plays a remarkable role in refining the structural features and other properties of the ferrite particles. The bulk density, porosity and lattice parameters of Ni-Zn ferrites were decreased with increased Al-content while the X-ray density was reduced. XRD patterns confirmed the single-phase cubic spinel structure of the ferrites particles. The room temperature infra-red spectra shows the features of higher and lower energy bands detected at ν_2 ~ 400-405 cm^{-1} and ν_1 ~ 590-594 cm^{-1}, respectively corresponded to tetrahedral (T-band) and octahedral vibration (O-band) complexes that also confirm the formation of Ni-Zn inverse spinels. The real part of the complex initial permeability, Curie temperature, ac resistivity and loss tangent of the ferrite powders were reduced while the quality factor was enhanced with the subsequent Al-substitution. The observed bi-layer space charge polarization feature was believed to correlate the normal dielectric behavior of Al-substituted Ni-Zn matrix.

Keywords: Ni-Al-Zn ferrites; surface morphology, permeability; Q-factor; loss tangent; AC resistivity.

1. Introduction

Spinel ferrites are one of the most important classes of magnetic materials that possess a multitude of technological applications such as electronic industries and information and communication technology. The uses of ferrites in many other areas are also constantly

increasing. The utility, variety, and versatility make them very useful and indispensable. Despite these applications, many other technological advances in a variety of areas have generated a growing demand for soft magnetic materials in many technical devices. Spinel ferrites enjoy a good combination of magnetic and insulating characteristics. They, generally, form a complex system comprised of grains, grain boundaries and pores. Physical and chemical properties of spinel ferrites also rely on other factors including the synthesis conditions, sintering temperatures, sintering time, rate of heating and cooling, and composition of the materials. They are preferred because of their high permeability and saturation magnetization in the radio-frequency (RF) region, electrical resistivity, mechanical hardness and chemical stability [1]. Ferrites are also efficient in obstructing and removing RF interference to audio systems [2]. It is to be noted that, in the recent past, a large number related researches have been carried out by different groups [3-6] and the references cited therein.

Over the years, the technology has been changing very quickly, and there has been an increasing need for the developing, controlling and diversification of electronic materials. Conductive natures of ferrites can meet this rapidly changing technology. Due to this large electrical resistivity, an applied alternating magnetic field will not induce eddy currents in ferrite materials which make ferrites ideal candidates for high frequency applications. Mixed Ni-Zn ferrites have been commercially utilized in radio frequency circuits, high quality filters, high resistive devices and transformer cores [7]. Relatively low permeability and higher bulk resistivity of Ni-Zn ferrites have found useful applications at high frequencies [8, 9]. The magnetic and dielectric behaviors of these ferrites depend on the distribution of these ions on tetrahedral and octahedral sites. The magnetization of either site can be reduced relative to the other one by replacing a non-magnetic ion such as Zn^{+2} in the corresponding site. The majority of technologically efficient materials having magnetic behavior like iron and soft magnetic alloys have low electrical resistivity which is not competent for high frequency applications. Due to the low electrical resistivity, a large amount of eddy currents were generated within the materials and thereby produced heat and waste energy [10, 11], which results to a poor materials performance.

Spinel based modern soft ferrites show various fascinating properties depending on their structural composition and cationic distributions [12]. Spinel ferrites are composed of two sub-lattices: tetrahedral, A-sites and octahedral (B-sites). In Ni–Zn ferrites, Ni and Zn ions

display sturdy preferences for B- and A- sites, respectively, but cationic replacements in the A- and B-sites can, generally, effectively improve their properties. The cationic replacement in these materials causes the redistribution of metal ions around A- and B-sites, as well as structural and surface morphological changes to their crystalline phase which results to substantial improvements in the magnetic and electrical properties [13-16]. For this reason, these ferrites gained a lot of attention in the theoretical and experimental research communities. A deep understanding of these modifications can provide us with valuable information on which these ferrites are suitable for their best applications. Moreover, ferrite particles with finer grains and well-ordered porosity are also beneficial to lower magnetic losses. Electrical and magnetic properties of Ni-Zn ferrites have been investigated by varying the nickel to zinc ratio, employing various manufacturing methods, annealing conditions and on the types and amounts of additives used [17, 18]. Hashim *et al*. [19] reported that Al-substituted Ni-Co ferrites demonstrate low eddy current losses, superior electrical resistivity, higher physical stability, square nature of hysteresis loops, and large saturation magnetization that are very important for high frequency technological applications. *To* date, several other studies have focused on understanding the impact of adding Al^{3+} ions onto the Ni-Zn system and have reported the reduction of charge transfer among Fe^{3+} and Fe^{2+} ions. Consequently, lower dielectric loss, improved saturation magnetization and higher resistivity were observed [20, 21].

Despite the fact that diamagnetic dopants in mixed ferrites play a great role in revising the crystalline structure and other properties of ferrite based materials, the mechanism associated with the enriched magnetic behavior is not clearly understood. Furthermore, structural studies of Al- substituted Ni-Zn ferrites *via* infrared spectrometry are very scant whereas the production of high quality ferrite particles with lower costs and low losses at high frequency for power applications is always a topic of study. Electrical properties of these materials provide us substantial information about the localized charge carriers that offer better realization of the dielectric behaviors while the Curie temperature and permeability studies contribute to understand the magnetic phenomenon associated in the presence of external alternating magnetic fields. Thus, extensive studies are needed to synthesize Ni–Zn ferrite particles with improved structural, magnetic, dielectric, transport and electrical properties. With this in mind, the present study is focused on investigating the structural features Ni-Al-

Zn ferrites *via* XRD, SEM, and FTIR spectroscopy, and incorporating them with the magnetic, dielectric and electrical properties.

2. Experimental details

2.1 Al substituted Ni-Zn ferrites preparation

Polycrystalline spinel ferrites with chemical formula $Ni_{0.65}Zn_{0.35}Al_xFe_{2-x}O_4$ (where x = 0 to 0.12 in steps of 0.03) were prepared by the standard double sintering ceramic method. An apposite proportion of raw materials (Fe_2O_3, NiO, ZnO and Al_2O_3) were weighed in accordance with their molecular weight and mixed circumstantially with the help of ball milling. To enhance the degree of mixing, milling was performed in a damp medium (de-ionized water). The pre-sintered powder was crushed thoroughly to make a finer powder. Small amounts like 2-3 drops of diluted polyvinyl alcohol were added up with resulting fine powder as a binder. From this sintered fine powder, samples with rod or plate shaped were made by utilizing a Universal Testing Machine (UTM). To prepare the sample pellets and toroids shapes, a pressure of 1.70 and 1.15 ton/cm^2 was applied via UTM. In the end, the pellets and toroids shaped samples were sintered for four hours at a constant temperature of 1200 ^{0}C in an air environment and allowed to cool inside the furnace. At the final level, the resulting samples were gradually heated to 650^{0}C in a programmable muffle furnace to avoid cracking in the finished samples. During this procedure, a constant heating rate of 5^{0}C/min was maintained.

2.2 Structural features and surface morphology

Structural identification and phase analysis of the ferrite particles were carried out by XRD studies using Phillips X'Pert PRO X-ray (PW3040) diffractometer. XRD measurements were performed by Cu-$K\alpha$ radiation (λ = 1.54178 Å) in the range of $2\theta = 20^0$ to 70^0 in the steps of 0.02^0. The samples were exposed to a primary beam operated at a power of 40 kV and 30 mA. All of the data of the samples was collected in a time gap of 1.0 s and were stored in the computer memory and analyzed by computer software "X'PERT HIGHSCORE".

The surface morphology studies of the Ni-Zn-Al ferrites were carried out using a PHILIPS XL 20 (Eindhoven, The Netherlands) scanning electron microscopic instrument. The SEM machine was operated at 25 kV. The elemental compositions of the Al-substituted Ni-Zn

ferrites was acquired by energy dispersive spectroscopy (EDX) unit attached to the SEM machine.

The infrared spectra for all the samples were recorded with FTIR spectrophotometer (Shimadzu FTIR Prestiage21) using KBr pellets in the wave number range of 2000-400 cm^{-1}.

2.3 Magnetic and dielectric properties of Ni-Al-Zn ferrites

The measurement of the permeability and Curie temperature of the toroidal samples were performed by Wayne Kerr 6500B Impedance Analyzer (Wayne Kerr Electronics Inc., USA). Pellet shaped sample of the Ni–Zn ferrite were made for the measurement of electrical as well as dielectric behaviours. Dielectric constant (ε′) and resistivity of the as prepared Ni–Zn ferrite samples was measured by HP impedance analyzer. Dielectric constants at varied frequency in the range of 0 - 10000 Hz were also performed at room temperature with the help of a laboratory made furnace.

2.4 Electrical properties of Ni-Al-Zn ferrites

The ac electrical resistivity measurements of the ferrite particles were conducted using 6500B Precision Magnetics Analyzer in the frequency range of 0 to 1000 Hz at a drive voltage of 0.5V at room temperature.

3. Results and discussion

3.1 XRD analysis

Structural characterizations and phase identification of Ni-Zn ferrites were carried out using the XRD technique *via* a Philips X'Pert Pro X-ray diffractometer. The Philips X'Pert Pro X-ray diffractometer uses Cu-K_α radiation (λ = 1.5406 Å). XRD patterns of Al-substituted Ni-Zn ferrites sintered at 1200°C have been presented in Figure 1. Single-phase cubic spinel structures of Ni-Zn ferrite particles were confirmed for all the samples. All the Ni-Zn ferrites display excellent crystallization together with well-defined diffraction lines. Five major diffraction peaks appeared at different planes of (220), (311), (400), (511) and (440) which is consistent with a spinel structure (JCPDS #08-0234). The appearance of these planes confirmed the existence of cubic spinel structures of Ni-Zn ferrite powers described in Ref. [22]. A single secondary phase detected at 2θ = 27.3° might have originated from a hematite (α-Fe_2O_4) phase (identified as H). It is also believed that the formation of this secondary

phase is a consequence of the preferential loss of Zn^{+2} ions during the sintering process. This is due to the fact that Zn is more volatile and at a lower Al-substitution in some ferrite and hematite samples, a few peaks are superimposed while at higher concentration these peaks are well resolved. This happens because the higher melting point of aluminum results in the incomplete conversion of Fe_2O_3 particle into ferrite phases [23].

Table 1 shows the variation of the lattice parameter of Ni-Zn ferrites as a function of substituent content *i.e.*, Al-content. This demonstrates that as the Al concentration increases, the lattice parameters of Ni-Zn ferrites are gradually decreased, thus obeying the Vegard's law and depending on the ionic radius and the cation distribution among the tetrahedral and the octahedral sites [24]. This decrement of lattice parameters is associated with the replacement of larger Zn^{2+} (8.7 nm) and Ni^{2+} (7.8 nm) ions by the smaller Al^{3+} (5.1 nm) ions. This variation in the lattice parameters can be also explained by the cation distribution: due to covalence effects, Zn^{2+} ions on the A-sites display a smaller ionic radius than on the B-sites. As a result, Al^{3+} ions possess a strong tendency to stay at tetrahedral B-sites by the replacement of Fe^{3+} ions at octahedral A-sites. It is also assumed that the smaller Al^{3+} ions result shrinking the Ni-Zn unit cell but the overall crystal symmetry is preserved. Similar phenomenon of lattice parameters of Al-substituted Ni-Zn ferrites were reported in an earlier study [25]. The porosity of Al-substituted Ni-Zn ferrites was calculated using the following equation, $P = \left(1 - \frac{d_B}{d_x}\right)$, where d_B is the bulk density obtained from the usual mass and dimensional consideration of the ferrite structures whereas X-ray density, d_x is defined as, $d_x = \frac{8M}{Na^3}$, where N is the Avogadro's number ($6.02 \times 10^{23} \text{mol}^{-1}$), and M is the molecular weight of the ferrites. The lattice parameters, bulk density, X-ray density and porosity values of Al-substituted Ni-Zn ferrites as estimated from XRD data are delineated in Table 1. Both the theoretical and bulk density values of Ni-Zn ferrites showed an incremental trend with the increase in Al-content. The X-ray density values vary between 5.31 to 5.37 g/cc while the bulk density values lie in the range of 4.96 to 4.79 g/cc. From Table 1 it is seen that the bulk density values are lower than the X-ray densities and the porosity of the as deposited Ni-Zn-Al ferrites and is gradually increased with the subsequent Al-substitution. This lower bulk density is related to the existence of pores, which were originated and developed in the course of heat treatment.

3.2 SEM and EDX analysis

The SEM was used to inspect the surface morphology of specimens at high magnification. Representative micrographs showing the surface morphology of Ni-Zn-Al ferrites with different Al-content are demonstrated in Fig. 2. SEM studies indicated that the average grain size of Ni-Al-Zn ferrites decreases with the increase of Al^{3+}-content. This leads to the fact that, as the Fe^{3+} ions are substituted by Al^{3+} ions, the potential changes in lattice parameter leads to the lattice strains. Consequently, internal stress is developed onto the ferrites samples that hinders the grain growths. Thus, the grain sizes of the Al-substituted Ni-Zn ferrites is reduced [21]. The elemental compositions of the Ni-Al-Zn ferrites determined by energy dispersive X-ray spectroscopy (EDX) are presented in Table 2. Estimated content (%) of the elements Zn, Ni, Al and O shown in Table 2 confirms that the ferrite samples are non-stoichiometric.

3.3 FTIR analysis

The FTIR analysis of Ni-Zn ferrites with progressive Al-substitution in the wave number range of 400 to 700 cm^{-1} shown in Figure 2, was carried out to acquire the structure information and to study the existence of chemical substances absorbed around the surface of the ferrite samples. As seen from Figure 2, bands detected at v_1 ~ 590-594 cm^{-1} and v_2 ~ 400-405 cm^{-1} corresponded to the vibration of the tetrahedral (T-band) and the octahedral (O-band) complexes respectively. FTIR results of Al-substituted Ni-Zn ferrites are summarized in Table 3. The existence of T- and O-bands in these wave number ranges confirms the development of the spinel phase of Ni-Zn ferrites which are an indication of the tetrahedral and octahedral structures as reported in the literature [26]. The high frequency absorption band v_1 is attributed to the intrinsic stretching vibrations of the A–O–A bonds, while the lower frequency band v_2 is ascribed to the metal stretching vibrations of the B–O–B bonds [27]. With the gradual increase in Al-substitution, both bands were slightly shifted towards the higher wave number sides. This is assumed to be due to the adjustment in the occupation of the cations in A-, and B-sites. Since the change in bond length is inversely related to the band frequency shift [28], consequently, the rise in absorption band frequency is associated with the reduction in A-, and B-bond lengths. Similar feature of pure expansion of the absorption bands associated with the cation distribution among A- and B-sites, *i.e.*, the formation of inverse spinels was reported in previous study [29].

3.4 Permeability studies

Figures 3 and 4 show that the complex initial permeability ($\mu^* = \mu' - i\,\mu''$, where μ' and μ'' are the real and imaginary parts of initial permeability [30]) of Al-incorporated Ni-Zn ferrites, as a function of frequency, in the frequency range of 10 kHz to 10 MHz. The μ' characterizes the energy deposited in the magnetic material from an external magnetic field, whereas the μ'' denotes the energy loss of the material. As observed in Figure 3, as the frequency is gradually increased, initial permeability values remained fairly invariant up to 1 MHz until the appearance of ferrimagnetic resonance and it then reduces at higher frequencies. The ferrimagnetic resonance occurs at a frequency known as the resonance frequency f_r, the regulating frequency of a ferrite material, below which the ferrite sample can be utilized [31]. Both the real and imaginary part of complex initial permeability is decreased after subsequent substitution with Al^{3+} ions. At the same time, the magnitude of the resonance frequency of Ni–Zn ferrites is increased as the Al-content is increased. This essentially shows that, the appropriate substitution of Al^{3+} ions onto the Ni–Zn ferrites can drive the magnetic permeability to a higher operating frequency, suggesting them to be promising candidates for applications to high-frequency devices. Initial permeability, μ_i of ferrites is defined by [32]: $\mu_i = \frac{M_S^2 D}{\sqrt{K_1}}$, where M_s is the saturation magnetization, D is the average crystallite size, and K_1 is the anisotropy constant. The variation in μ_i is mainly triggered by the differences in the crystallite sizes and magnetocrystalline anisotropy constants of ferrite particles. Generally, the anisotropy constants depend on the nature and the amount of the substitutions. Since, the anisotropy constant varies with the change in Fe^{2+} ions concentration, the gradual increase in Al-content, the number of Fe^{3+} ions available to interact with the Ni^{2+} ions and formation of Fe^{2+} ions is reduced. As a result, the permeability is gradually declined with the substitution of Al-content.

Table 1 indicates that the bulk density of Ni-Zn ferrites decreases with the increase in Al-content, and as a result, the grain sizes of the samples should also decrease and thereby a decline is permeability is to be expected. It is established that the permeability values of polycrystalline ferrites is associated with the combination of two mechanisms: spin rotation and domain wall motion [33, 34]. Grain size lowering results in a reduction of permeability and a lower contribution from the domain walls, while the density reduction of the material is

correlated to a lower contribution from domain wall displacement. Apart from crystallite size, the existence of pores also influences the initial permeability. Pores, generally, impede the domain wall motion by trapping them around; consequently, the volume swept by the domain walls in the presence of applied magnetic field is reduced. As a result the initial permeability values are lowered [35].

The permeability values of ferrite particles strongly depend on the number of Fe^{3+} ions in the B-sites. In Ni-Zn ferrites, the Al^{3+} ions which entered into the B-sites are replaced for Fe^{3+} ions. As a consequence, the saturation magnetization is reduced, thereby decreasing the permeability of the Ni-Zn ferrites, because the initial permeability is proportional to the square of saturation magnetization. It is also believed that as the Al is added to Ni-Zn ferrites, it forms aluminium iron oxides and segregates around the grain boundaries pining at the domain wall. As a result, domain wall energy is enlarged and the permeability values are reduced [36]. Furthermore, the intragranular pores may be the cause of the pining of the domain walls that result to drop of magnetic behaviours of Ni-Zn ferrites [37].

3.5 Curie temperature studies

The Curie temperature data of Al-substituted Ni-Zn ferrites estimated from permeability measurements are shown in Figure 5 and Table 4. From Figure 5 and Table 4, it is observed that the T_c values of Ni-Zn ferrites are monotonically decreased with the systematic increase in Al-content to Ni-Zn matrix. In Ni–Zn ferrites, T_c depends on the magnitude of A–B super-exchange interaction (Fe_A^{3+}–O^{2-}–Fe_B^{3+}) in which the interaction between iron ions plays a prominent role [38]. Generally, the Curie temperature gives an indication of the amount of energy required to overcome the long-range ordering in the ferromagnetic materials and may be explained by modification of the A-B exchange interaction. It is well known that in ferrite particles, the A-B exchange interaction is due to the alteration of the ionic distributions between A and B sites when non-magnetic Al^{3+} ions are incorporated. The non-magnetic Al^{3+} ions preferentially occupy octahedral B-sites replacing an equivalent amount of the magnetic Fe^{3+} ions from the octahedral A-sites. The replacement of Fe^{3+} ions with Al^{3+} ions, generally, reduces the net magnetic moment on A-sites followed by the dilution of the A–B exchange interaction which induces the drop of the T_c values of Ni-Zn ferrites. Thus the thermal

energy, kT_c needed to counterbalance the spin alignment is reduced and the Curie temperature falls off.

3.6 Q-factor of Ni-Zn ferrites

Variations of the relative *Q*-factor of Al- substituted Ni-Zn ferrites as a function of frequency are shown in Figure 6. Figure 6 shows the relative Q-factor gently rising up with the rise in frequency reaching to a highest value at a particular frequency, f_r = 1.1 MHz and then decreasing linearly with the further increase in frequency. It also shows that at lower and higher frequency regions, the relative Q-factor does not show any remarkable changes with the subsequent increase in the substituent content while at the mid frequency range it reduces monotonically with the continuous increase in Al-content. On an analysis of the frequency response Q-factor data, an ideal frequency range can be seen at which these materials exhibit superior device performance with lower energy loss. It is established that for low frequency applications, materials with low Q-factor execute superior filters performances which are used to reduce undesirable oscillations and the high frequency content of rapidly passing signals. They are well-known as reducing ringing at high frequency applications. Usually, in ferrites the loss tangent is associated to various domain defects, hysteresis loss, eddy current loss, and residual loss [39]. Generally, the eddy current losses in ferrites can be successfully reduced by increasing the resistivity, while the hysteresis loss and residual loss can be decreased by eliminating possible impurities in the precursor materials and minimizing the domain wall relaxation, respectively [40]. All these factors become operative when the real part of initial complex permeability starts to fall around the resonance frequency [41]. At resonance condition, the maximum energy is transferred from the external magnetic field to the crystal lattice, consequently there is a sharp drop in relative Q-factor. The highest Q-factor of 5900 was recorded for the undoped Ni-Zn ferrites.

3.7 Loss tangent of Ni-Zn ferrites

The variation of loss tangent of Al-substituted Ni-Zn ferrites with frequencies is shown in Figure 7. From Figure 7, it is seen that the loss tangent declines rapidly at lower frequency regions whereas at the high frequency sides the loss tangent become almost frequency independent. It is clearly seen that loss tangent values of Ni-Zn ferrites decrease with the

increase in frequency and display normal dispersion behaviour in the low frequency regions. This phenomenon can be shown on the basis of the space charge polarization concept: ferrites comprising of conducting grains are differentiated by exceedingly high resistive grain boundaries [42]. The resulting peaks are due to more than one equilibrium position of the metallic ions such as two adjacent octahedral sites around spinel phase. These octahedral sites have the same potential energy differentiated by a potential wall which generates a possibility for the ions to pass through from one equilibrium site to another [43]. Accordingly, it's possible for ions to exchange their locations between the two equilibrium states with a certain specific frequency known as the natural frequency of jump between these states. Similar results were reported in earlier studies with Al^{3+}-substituted spinel ferrites [44-46]. It is also established that higher loss tangents at lower frequency sides arises due to the interfacial type of polarization [47]. This is because the high resistive grain boundaries are effective at low frequencies, and a greater amount of energy is essential for the electron transfer between the Fe^{2+} and Fe^{3+} ions and a high loss is expected. However at high frequency regions, generally, the losses are lower due to the hindrance of domain wall motion and the magnetization is forced to change by rotation [48]. The reduction of loss tangent at higher frequencies is also related to the relaxation phenomena of the magnetization of domain walls [49]. Higher frequency sides correspond to lower resistive grains and less energy is needed for electron exchange between Fe^{2+} and Fe^{3+} ions at the B-sites. The loss tangent is influenced by several factors such as stoichiometry, Fe^{2+} ions concentration and structural homogeneity. Similar behavior of dielectric loss has been previously reported in nanocrystalline ferrites [50]. The maximum loss tangent arises when the hopping frequency of electrons between Fe^{3+} and Fe^{2+} becomes equal to the frequency of the applied electric field that is the maximum amount of energy is transported to the electrons [51, 52].

In ferrite materials, the dielectric loss arises because of the lag in polarization with respect to the external electric field. When the frequency of the applied field corresponds to the hopping frequency of the charge carriers, the greatest amount of energy is imparted to the vibrating charge carriers and a sharp peak is detected. It is also known that in ferrites the loss tangent arises from the non-uniform domain wall movements, domain defects, variations in flux densities and domain wall extinctions [53]. The loss tangent characterizes the energy loss within the dielectric medium at different frequencies and is the central part of the total core

loss in ferrite materials. This means for low core loss, low dielectric losses are required in real life applications of these samples [54].

3.8 AC resistivity of Ni-Zn ferrites

AC resistivity data of Al-substituted Ni-Zn ferrites, conducted in the frequency range of 1 kHz to 10^3 kHz at room temperature, are shown in Figure 8. It is evident that the ac electrical resistivity of Al- substituted Ni-Zn ferrites is gradually decreased with the rise in frequency of the applied ac electric field and progression of Al-content, and at high frequency sides become fairly invariant. All the curves exhibit substantial dispersion with the change in frequency, which is an important characteristic of ferromagnetic materials. We conclude that at low frequency regions these ferrites exhibit a lower eddy current loss due to the fact that resistivity of ferrites is inversely proportional to the eddy current loss. The increase in frequency boosts the hopping frequency of charge carriers and thereby causes an increase in the conduction process. As a result of the improved conduction process, the resistivity is significantly reduced. The electron interchange between $Ni^{2+} + Fe^{3+} \leftrightarrow Fe^{2+} + Ni^{3+}$ ions around the neighboring octahedral B-sites is responsible for the conduction process in ferrite particles. As described herein (See section 3.6), the frequency reliance of ac electrical conductivity is assumed to obey the Maxwell–Wanger double-layer model for ferrites. In this theory, the first layer is formed with a large number of fairly conducting Fe^{2+} ions separated by a thin and highly resistive grain boundaries [55]. In lower frequency regions, the grain boundaries are more effective and the jumping frequency of electrons between Fe^{2+} and Fe^{3+} ions become very limited. However, as the frequency is raised, the conductive grains are assumed to be more active and thereby allowing the transfer of electrons between Fe^{2+} and Fe^{3+} ions. Consequently, ac electrical conductivity is increased with the increase in frequency [55]. Ni–Zn ferrites crystallized into mixed spinel structures where Fe^{3+} ions are dispersed between A- and B-sites, whereas Ni^{2+} and Zn^{2+} ions exist at A- and B-sites respectively. In metal oxides having ions of a given element in more than one valence state, electronic conduction occurs due to the transfer of electrons between Fe^{3+} and Fe^{2+} ions around the octahedral sites without any change in the energy state of the crystalline state[56]. The possibility of electron jumping is higher at the B-sites because the distance between the metal ions in the B-sites (29.6 nm) is relatively smaller than that of the A-sites (36.3 nm) [57]. As a result, the electronic conduction is increased if the concentrations of Fe^{2+} ions become

greater. Furthermore, the potential existence of Ni^{3+} ions around B-sites might also add some value to the conductivity by transporting electrons within $Ni^{2+} \leftrightarrow Ni^{3+}$ ions.

4. Conclusions

Ceramic Ni-Zn ferrities with progressive Al-substitution have been studied for their phase identification, infrared structural, and other properties. Al-substitution plays an important role in refining the physical, structural, dielectric and other supplimentary propertities of Ni-Zn ferrite system. The bulk density, porosity and lattice constants were linearly decreased with the increase in Al-content while the X-ray density was increased. The XRD studies offered the confirmation of the single-phase cubic spinel assembly of the ferrite powders without having any other transitional structures. Existence of T-bands and O-bands were confirmed *via* room temperature FTIR studies. Frequency stability of the real part of the initial complex permeability was increased with the continuing increase in Al-content. Similar to dielectric features, the ac electrical conductivity was also assumed to follow double-layer space charge phenomenon. The electronic conduction is associated with the relocation of electrons between Fe^{3+} and Fe^{2+} ions around B-sites without any change in the energy state of the crystalline state.

Acknowledgements

One of the authors (T.K. Bromho) gratefully acknowledges the financial support of Jahangirnagar University. M. Mahbubur Rahman also acknowledges the support provided by Jahangirnagar University. Khalil Ibrahim is gratefully acknowledging the financial support of Iraqi Government. Kamrul Hasan gratefully acknowledges the Seed Research Project (1602142021-P), and Organometallic Research Group, University of Sharjah. Zhong-Tao Jiang is supported by the Murdoch University.

References

[1] E. Olsen, J. Thonstad, Nickel ferrite as inert anodes in aluminium electrolysis: Part I Material fabrication and preliminary testing, Journal of Applied Electrochemistry, 29 (1999) 293-299.

[2] C.O. Augustion, D. Prabhakaran, L.K. Srinivasan, Fabrication and characterization of NiCr2O4 spinel, Journal of Materials Science Letters, 12 (1993) 383-386.

[3] M. Ashtar, A. Munir, M. Anis-ur-Rehman, A. Maqsood, Effect of chromium substitution on the dielectric properties of mixed Ni-Zn ferrite prepared by WOWS sol–gel technique, Materials Research Bulletin, 79 (2016) 14-21.

[4] A.I. Borhan, A.R. Iordan, M.N. Palamaru, Correlation between structural, magnetic and electrical properties of nanocrystalline Al3+ substituted zinc ferrite, Materials Research Bulletin, 48 (2013) 2549-2556.

[5] I.H. Gul, E. Pervaiz, Comparative study of $NiFe_{2-x}Al_xO_4$ ferrite nanoparticles synthesized by chemical co-precipitation and sol–gel combustion techniques, Materials Research Bulletin, 47 (2012) 1353-1361.

[6] S.S. Kumbhar, M.A. Mahadik, V.S. Mohite, Y.M. Hunge, K.Y. Rajpure, C.H. Bhosale, Effect of Ni content on the structural, morphological and magnetic properties of spray deposited Ni–Zn ferrite thin films, Materials Research Bulletin, 67 (2015) 47-54.

[7] T. Suzuki, T. Tanaka, K. Ikemizu, High density recording capability for advanced particulate media, Journal of Magnetism and Magnetic Materials, 235 (2001) 159-164.

[8] G.F. Dionne, R.G. West, Magnetic and dielectric properties of the spinel ferrite system $Ni_{0.65}Zn_{0.35}Fe_{2-x}Mn_xO_4$, Journal of Applied Physics, 61 (1987) 3868-3870.

[9] S. Hilpert, B. Deutseh, The structures and origins of magnetic properties of ferrites and iron oxides, Chem. Ges., 42 (1909) 2248-2261.

[10] P.C.R. Varma, R.S. Manna, D. Banerjee, M.R. Varma, K.G. Suresh, A.K. Nigam, Magnetic properties of $CoFe_2O_4$ synthesized by solid state, citrate precursor and polymerized complex methods: A comparative study, Journal of Alloys and Compounds, 453 (2008) 298-303.

[11] S. Seifikar, A. Tabei, E. Sachet, T. Rawdanowicz, N. Bassiri-Gharb, J. Schwartz, Growth of (111) oriented $NiFe_2O_4$ polycrystalline thin films on Pt (111) via sol-gel processing, Journal of Applied Physics, 112 (2012) 063908.

[12] Z.H. Khan, M. Mahbubur Rahman, S.S. Sikder, M.A. Hakim, D.K. Saha, Complex permeability of Fe-deficient Ni–Cu–Zn ferrites, Journal of Alloys and Compounds, 548 (2013) 208-215.
[13] A.M. El-Sayed, Electrical conductivity of nickel–zinc and Cr substituted nickel–zinc ferrites, Materials Chemistry and Physics, 82 (2003) 583-587.
[14] S.K. Nath, M.M. Rahman, S.S. Sikder, M.A. Hakim, S.M. Hoque, Magnetization and Magnetic Behavior of $Ni_{1-x}Cd_xFe_2O_4$ Ferrites, ARPN Journal of Science and Technology, 3 (2013) 106-111.
[15] S. Pervin, M.M. Rahman, F. Ahmed, M.A. Hakim, Investigation of magnetic, dielectric and electrical properties of Ba-hexaferrites, Indian Journal of Physics, 86 (2012) 1065-1072.
[16] M.M. Rahman, P.K. Halder, F. Ahmed, T. Hossain, M. Rahaman, Effect of Ca-substitution on the Magnetic and Dielectric Properties of Mn-Zn Ferrites, Journal of Scientific Research, 4 (2012) 297-306.
[17] C. Caizer, M. Stefanescu, Magnetic characterization of nanocrystalline Ni-Zn ferrite powder prepared by the glyoxylate precursor method, Journal of Physics D: Applied Physics, 35 (2002) 3035-3040.
[18] D. Guo, Z. Zhang, M. Lin, X. Fan, G. Chai, Y. Xu, D. Xue, Ni-Zn ferrite films with high resonance frequency in the gigahertz range deposited by magnetron sputtering at room temperature, Journal of Physics D: Applied Physics, 42 (2009) 125006.
[19] M. Hashim, Alimuddin, S. Kumar, B.H. Koo, S.E. Shirsath, E.M. Mohammed, J. Shah, R.K. Kotnala, H.K. Choi, H. Chung, R. Kumar, Structural, electrical and magnetic properties of Co–Cu ferrite nanoparticles, Journal of Alloys and Compounds, 518 (2012) 11-18.
[20] B.R. Babu, K.V. Ramesh, M.S. Prasad, Y. Purushotham, Study of microstructure and augmentation of DC electrical resistivity due to Al3+ substitution in Ni–Zn nano ferrite system synthesized via auto combustion, Modern Physics Letters B, 29 (2015) 1550151.
[21] I. Maghsoudi, H. Shokrollahi, M.J. Hadianfard, J. Amighian, Synthesis and characterization of $NiAl_xFe_{2-x}O_4$ magnetic spinel ferrites produced by conventional method, Powder Technology, 235 (2013) 110-114.
[22] P.G. Hewitt, Conceptual Physics, 7th ed., Harper Collins College Publishers, New York, USA, 1993.
[23] B.P. Rao, K.H. Rao, Distribution of In^{3+} ions in indium-substituted Ni–Zn–Ti ferrites, Journal of Magnetism and Magnetic Materials, 292 (2005) 44-48.
[24] N. Rezlescu, E. Rezlescu, Nickel-zinc ferrites with additives for use in magnetic heads, Ceramics International, 13 (1987) 131-132.

[25] K.V. Kumar, D. Paramesh, P.V. Reddy, Effect of aluminium doping on structural and magnetic properties of Ni-Zn ferrite nanoparticles, World Journal of Nano Science and Engineering, 5 (2015) 68-77.
[26] R.D. Waldron, Infrared Spectra of Ferrites, Physical Review, 99 (1955) 1727-1735.
[27] G.D. Tang, Z.F. Shang, X.Y. Zhang, J. Xu, Z.Z. Li, C.M. Zhen, W.H. Qi, L.L. Lang, Evidence from infrared spectra for the magnetic moment directions of CR cations in the spinel ferrites, Physica B: Condensed Matter, 463 (2015) 26-29.
[28] V.K. Lakhani, T.K. Pathak, N.H. Vasoya, K.B. Modi, Structural parameters and X-ray Debye temperature determination study on copper-ferrite-aluminates, Solid State Sciences, 13 (2011) 539-547.
[29] R.S. Yadav, J. Havlica, M. Hnatko, P. Šajgalík, C. Alexander, M. Palou, E. Bartoníčková, M. Boháč, F. Frajkorová, J. Masilko, M. Zmrzlý, L. Kalina, M. Hajdúchová, V. Enev, Magnetic properties of $Co_{1-x}Zn_xFe_2O_4$ spinel ferrite nanoparticles synthesized by starch-assisted sol-gel autocombustion method and its ball milling, Journal of Magnetism and Magnetic Materials, 378 (2014) 190-199.
[30] E. Rezlescu, N. Rezlescu, C. Pasnicu, M.L. Craus, D.P. Popa, The influence of additives on the properties of Ni-Zn ferrite used in magnetic heads, Journal of Magnetism and Magnetic Materials, 117 (1992) 448-454.
[31] H. Su, H. Zhang, X. Tang, Y. Jing, Z. Zhong, Complex permeability and permittivity spectra of polycrystalline Ni-Zn ferrite samples with different microstructures, Journal of Alloys and Compounds, 481 (2009) 841-844.
[32] M. Siva Ram Prasad, B.B.V.S.V. Prasad, B. Rajesh, K.H. Rao, K.V. Ramesh, Magnetic properties and DC electrical resistivity studies on cadmium substituted nickel–zinc ferrite system, Journal of Magnetism and Magnetic Materials, 323 (2011) 2115-2121.
[33] N. Rezlescu, E. Rezlescu, C. Pasnicu, M.L. Craus, Effects of the rare-earth ions on some properties of a nickel-zinc ferrite, Journal of Physics: Condensed Matter, 6 (1994) 5707.
[34] G.F. Dionne, A review of ferrites for microwave applications, Proceedings of the IEEE, 63 (1975) 777-789.
[35] R. Valenzuela, Magnetic Ceramics, Cambridge University Press, Cambridge, UK, 1994.
[36] J. Smith, H.P.J. Wijn, Ferrites, Philips Technical Library, Eindhoven, The Netherlands, 1959.
[37] L.G.V. Uitert, dc Resistivity in the Nickel and Nickel Zinc Ferrite System, The Journal of Chemical Physics, 23 (1955) 1883-1887.

[38] T. Tsutaoka, Frequency dispersion of complex permeability in Mn-Zn and Ni-Zn spinel ferrites and their composite materials, Journal of Applied Physics, 93 (2003) 2789-2796.
[39] M.A. Rahman, M.A. Rahman, A.K.M.A. Hossain, Effect of Cu^{2+} substitution on structural, magnetic and transport properties of $Fe_{2.5}Zn_{0.5-x}Cu_xO_4$, Journal of Magnetism and Magnetic Materials, 369 (2014) 168-175.
[40] S.S. Bellad, B.K. Chougule, Composition and frequency dependent dielectric properties of Li-Mg-Ti ferrites, Materials Chemistry and Physics, 66 (2000) 58-63.
[41] F.G. Brockman, P.H. Dowling, W.G. Steneck, Dimensional effects resulting from a high dielectric constant found in a ferromagnetic ferrite, Physical Review, 77 (1950) 85-93.
[42] C.G. Koops, On the dispersion of resistivity and dielectric constant of some semiconductors at audiofrequencies, Physical Review, 83 (1951) 121-124.
[43] M. Ashtar, A. Munir, M. Anis-Ur-Rehman, A. Maqsood, Effect of chromium substitution on the dielectric properties of mixed Ni-Zn ferrite prepared by WOWS sol-gel technique, Materials Research Bulletin, 79 (2016) 14-21.
[44] M. Ahmad, R. Grössinger, I. Ali, I. Ahmad, M.U. Rana, Synthesis and characterization of al-substituted W-type hexagonal ferrites for high frequency applications, Journal of Alloys and Compounds, 577 (2013) 382-388.
[45] K.M. Batoo, S. Kumar, C.G. Lee, Alimuddin, Influence of Al doping on electrical properties of Ni-Cd nano ferrites, Current Applied Physics, 9 (2009) 826-832.
[46] S. Verma, J. Chand, M. Singh, Mössbauer, magnetic, dielectric and dc conductivity of Al3+ ions substituted Mg-Mn-Ni nano ferrite synthesized by citrate precursor method, Advanced Materials Letters, 4 (2013) 310-316.
[47] P.A. Shaikh, R.C. Kambale, A.V. Rao, Y.D. Kolekar, Studies on structural and electrical properties of $Co_{1-x}Ni_xFe_{1.9}Mn_{0.1}O_4$ ferrite, Journal of Alloys and Compounds, 482 (2009) 276-282.
[48] D.R. Secrist, H.L. Turk, Electrical Properties of High-Density Iron-Deficient Nickel-Zinc Ferrites, Journal of the American Ceramic Society, 53 (1970) 683-686.
[49] L. Hongying, Z. Haifeng, Y. Lanying, X. Jijing, G. Shucai, M. Jian, H. Guangyan, Preparation and Characterization of W-Type Hexaferrite Doped with La^{3+}, Journal of Rare Earths, 25 (2007) 590-595.
[50] K.M. Batoo, S. Kumar, C.G. Lee, Alimuddin, Finite size effect and influence of temperature on electrical properties of nanocrystalline Ni–Cd ferrites, Current Applied Physics, 9 (2009) 1072-1078.

[51] M. Ajmal, N.A. Shah, A. Maqsood, M.S. Awan, M. Arif, Influence of sintering time on the structural, electrical and magnetic properties of polycrystalline $Cu_{0.6}Zn_{0.4}Fe_2O_4$ ferrites, Journal of Alloys and Compounds, 508 (2010) 226-232.
[52] N. Singh, A. Agarwal, S. Sanghi, Dielectric relaxation, conductivity behavior and magnetic properties of Mg substituted Zn-Li ferrites, Current Applied Physics, 11 (2011) 783-789.
[53] P.B. Konstantin, E.P. Svirina, The Hall Effect in Ferrites, Soviet Physics Uspekhi, 11 (1969) 620.
[54] I.H. Gul, A. Maqsood, M. Naeem, M.N. Ashiq, Optical, magnetic and electrical investigation of cobalt ferrite nanoparticles synthesized by co-precipitation route, Journal of Alloys and Compounds, 507 (2010) 201-206.
[55] J.S. Ghodake, R.C. Kambale, S.V. Salvi, S.R. Sawant, S.S. Suryavanshi, Electric properties of Co substituted Ni-Zn ferrites, Journal of Alloys and Compounds, 486 (2009) 830-834.
[56] J.H. De Boer, E.J.W. Verwey, Semi-conductors with partially and with completely filled 3d-lattice bands, Proceedings of the Physical Society, 49 (1937) 59-71.
[57] V.K. Babbar, J.S. Chandel, S.P. Sud, Low loss Ni-Sn-Al ferrites for high frequency applications, Journal of Materials Science Letters, 14 (1995) 763-765.

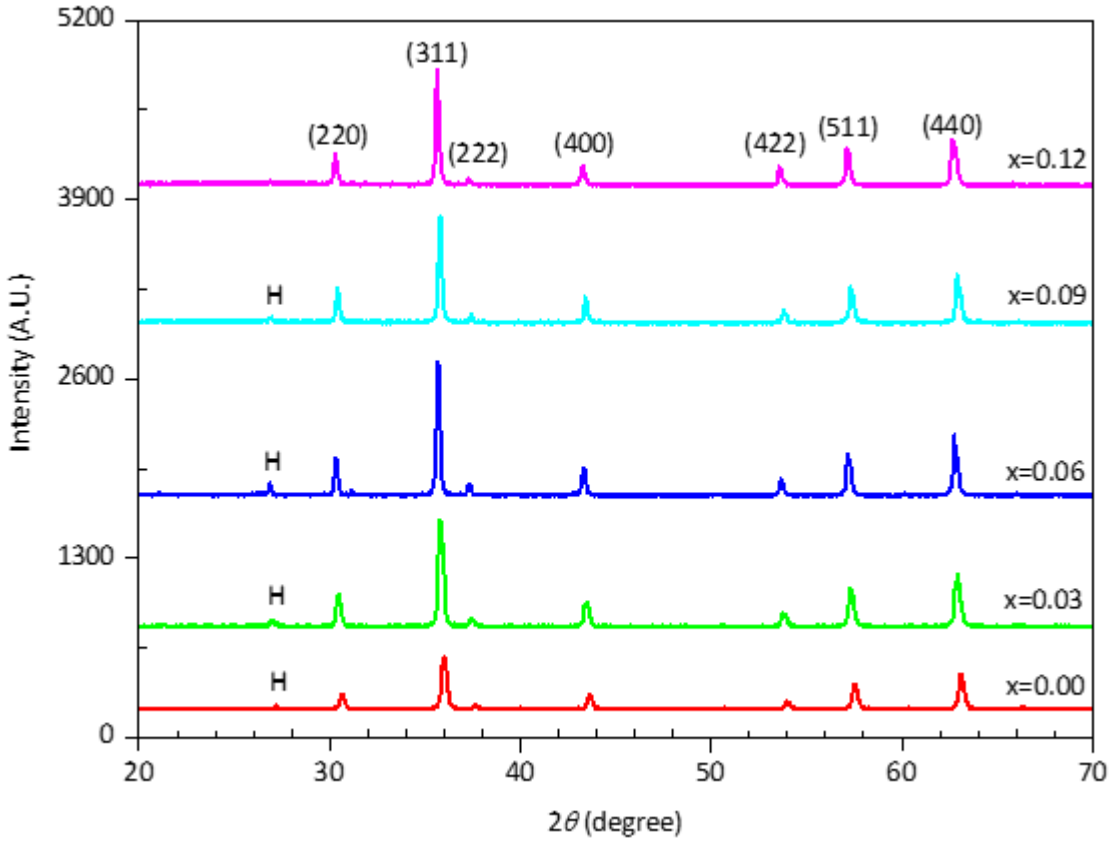

Fig. 1. XRD patterns of $Ni_{0.65}Zn_{0.35}Al_xFe_{2-x}O_4$ferrites with different Al content.

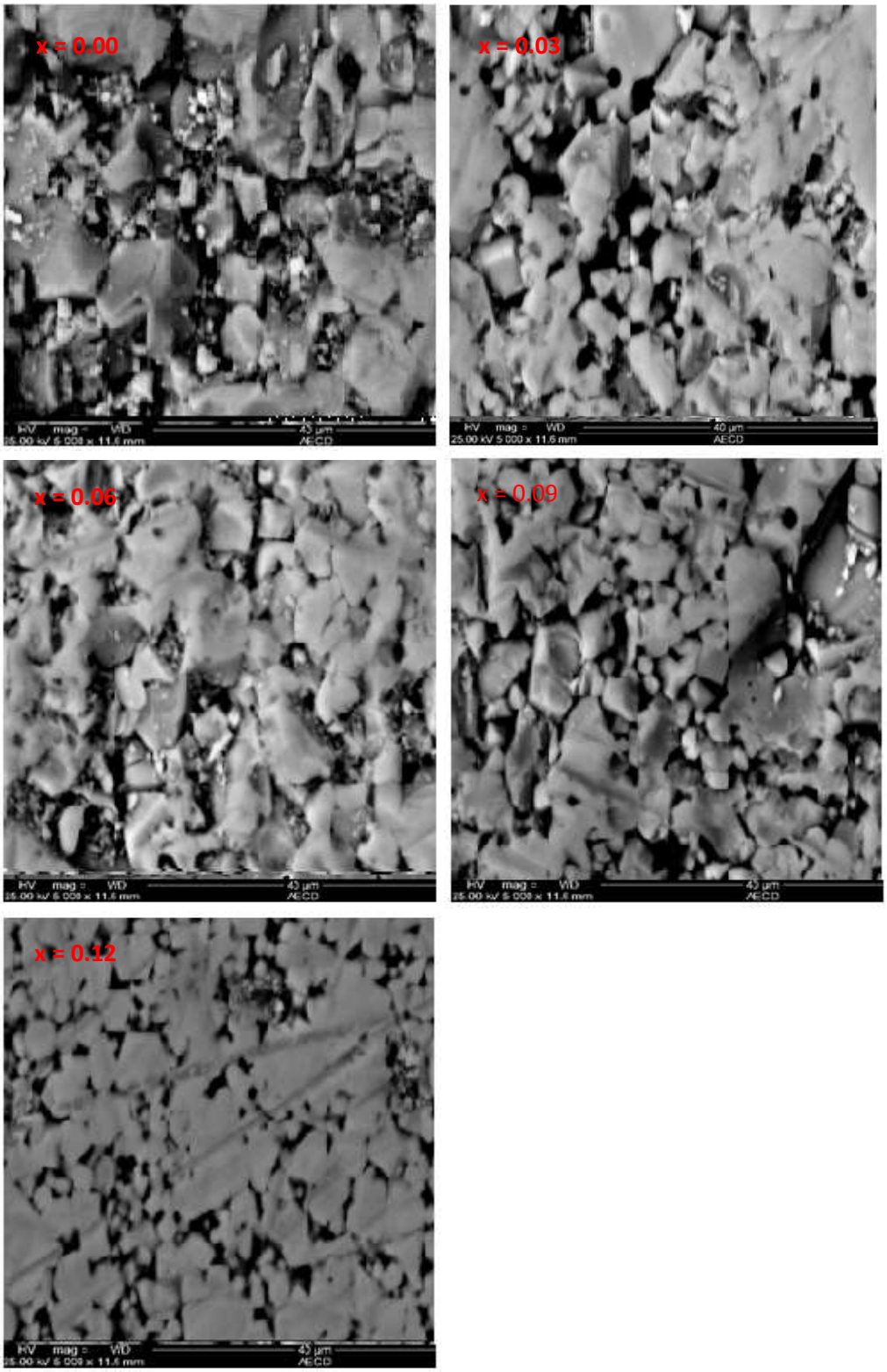

Fig. 2. The SEM micrographs of $Ni_{0.65}Zn_{0.35}Al_xFe_{2-x}O_4$ at various aluminum contents.

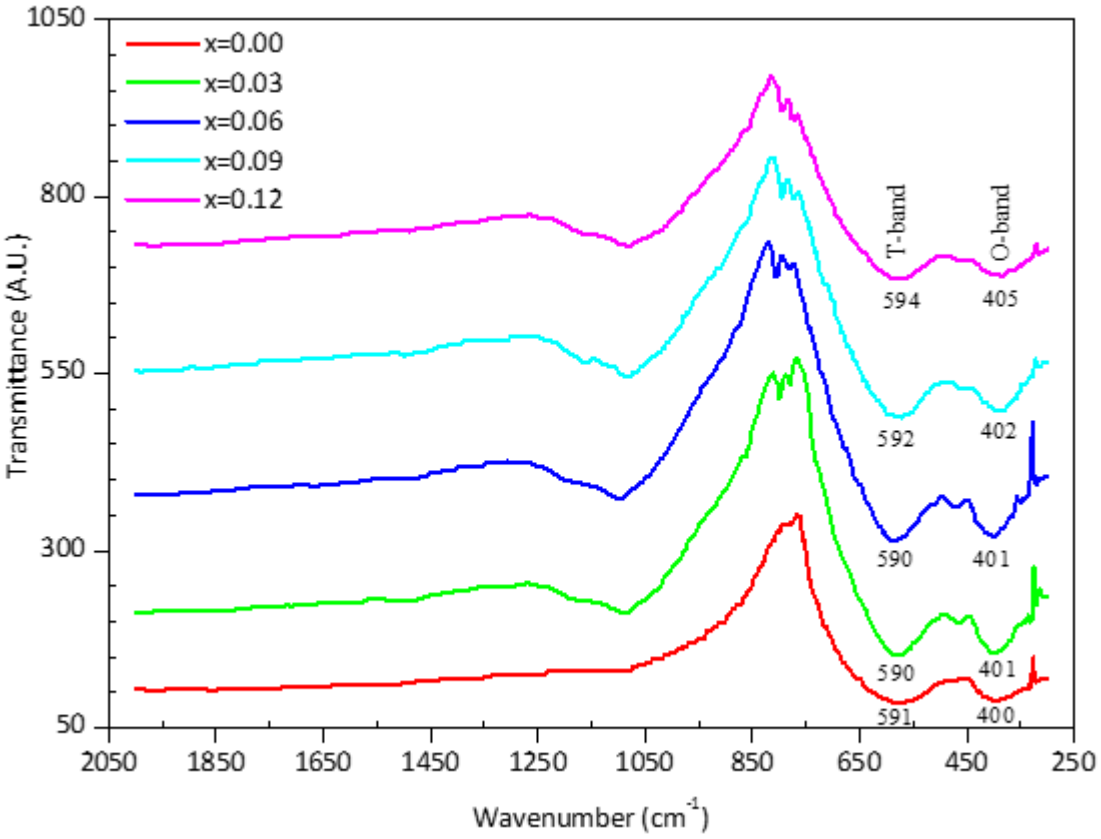

Fig. 3. FTIR spectra of $Ni_{0.65}Zn_{0.35}Al_xFe_{2-x}O_4$, where x = 0, 0.03, 0.06, 0.09, 0.12 ferrites.

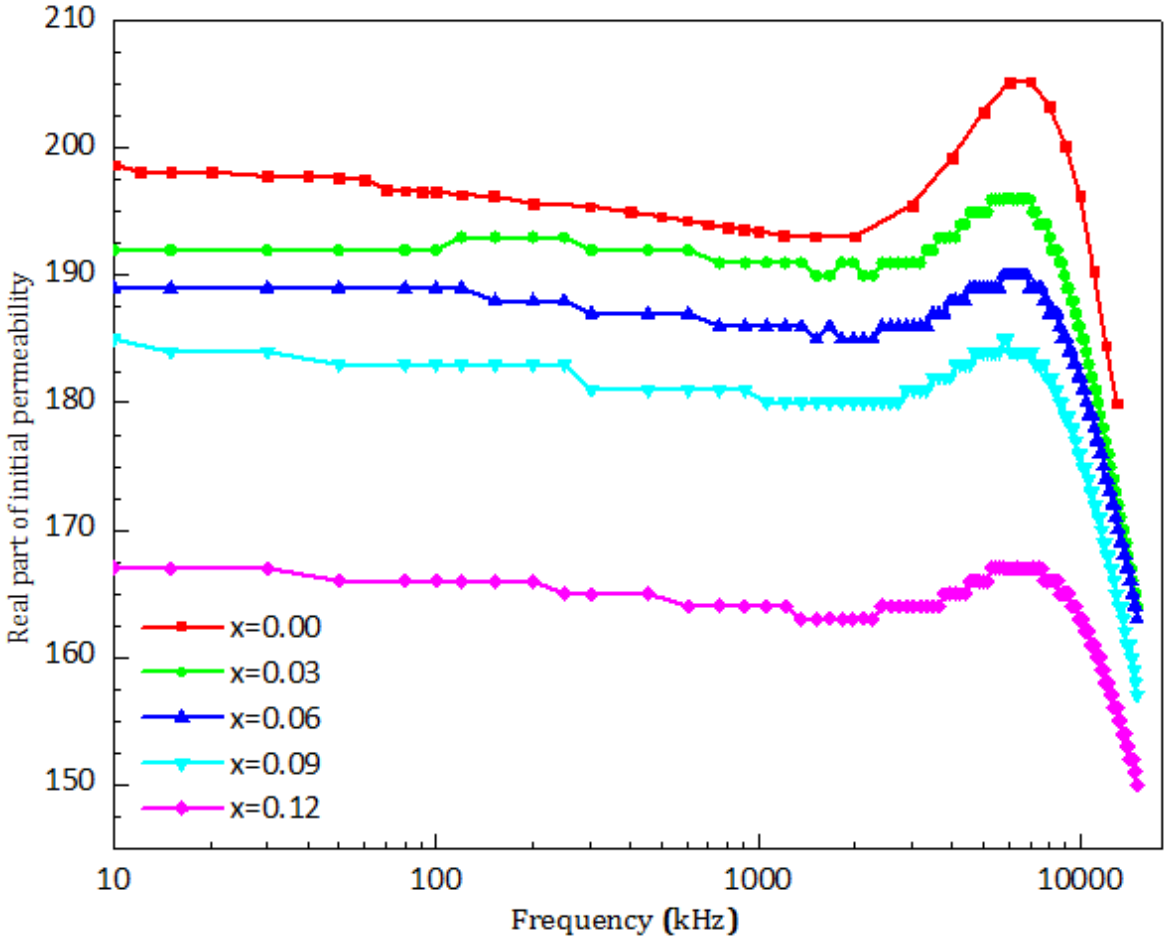

Fig. 4. Frequency dependence real part of initial permeability spectra of $Ni_{0.65}Zn_{0.35}Al_xFe_{2-x}O_4 (x = 0,\ 0.03, 0.06, 0.09,\ 0.12)$ ferrites.

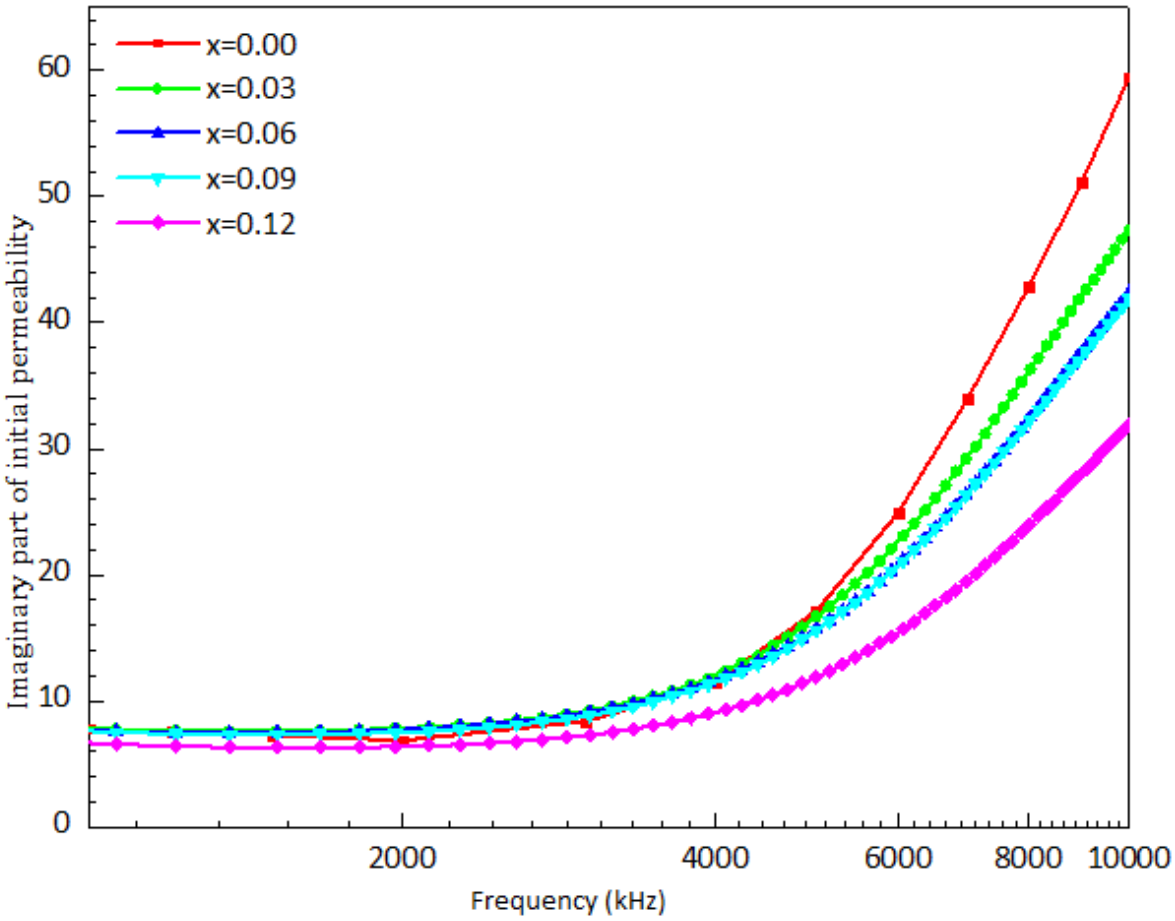

Fig. 5. Frequency dependence imaginary part of initial permeability spectra of $Ni_{0.65}Zn_{0.35}Al_xFe_{2-x}O_4 (x = 0,\ 0.03, 0.06, 0.09,\ 0.12)$ ferrites.

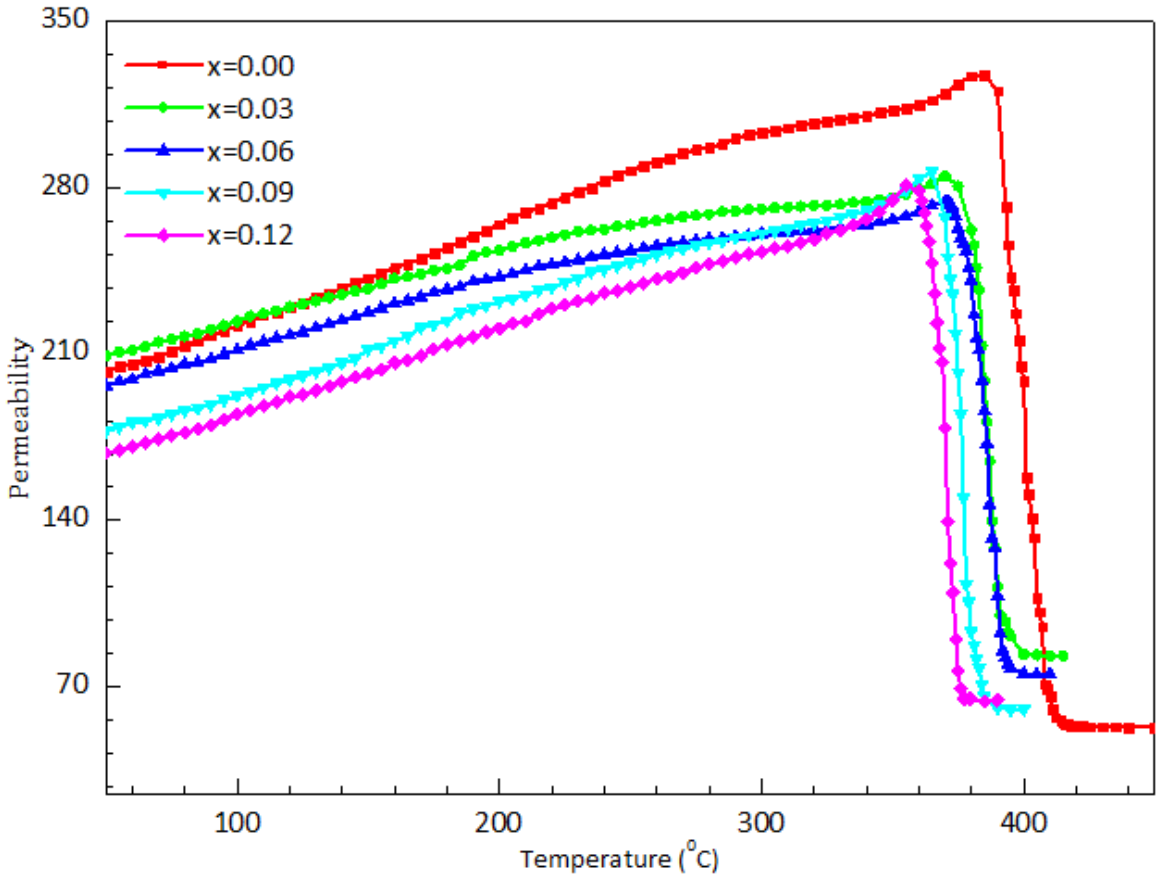

Fig. 6. Curie temperature estimation of $Ni_{0.65}Zn_{0.35}Al_xFe_{2-x}O_4$($x$ = 0, 0.03, 0.06, 0.09, 0.12) ferrites.

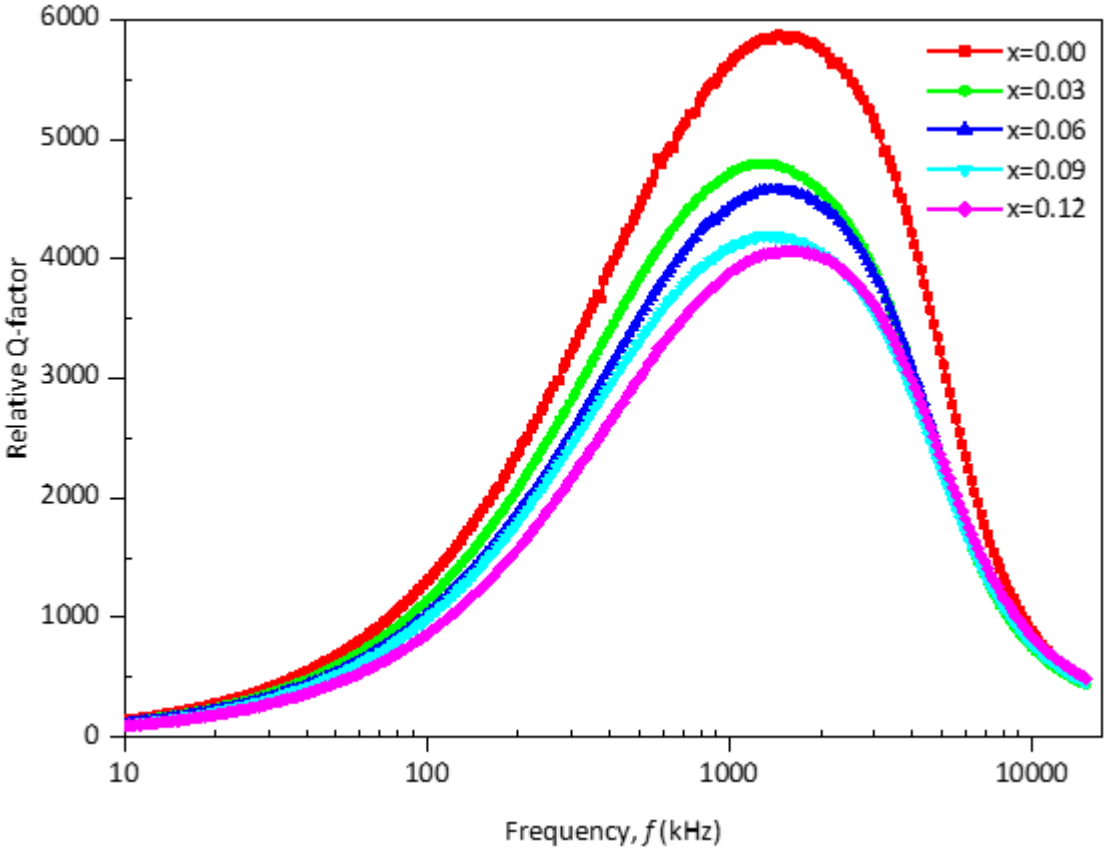

Fig. 7. The variation of relative Q-factor of $Ni_{0.65}Zn_{0.35}Al_xFe_{2-x}O_4$ (x = 0, 0.03, 0.06, 0.09, 0.12) ferrites with frequency.

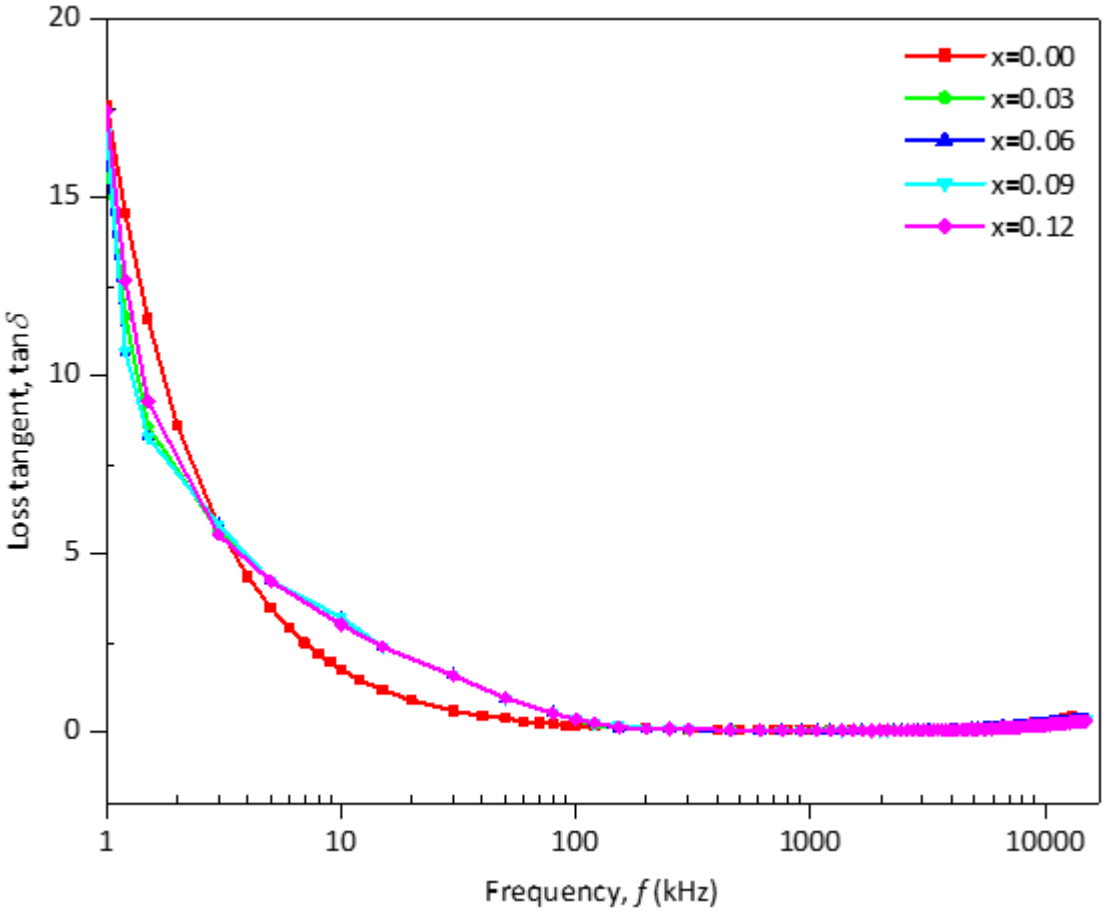

Fig. 8. The variation of loss tangent with frequency of $Ni_{0.65}Zn_{0.35}Al_xFe_{2-x}O_4$ (x = 0, 0.03, 0.06, 0.09, 0.12) ferrites.

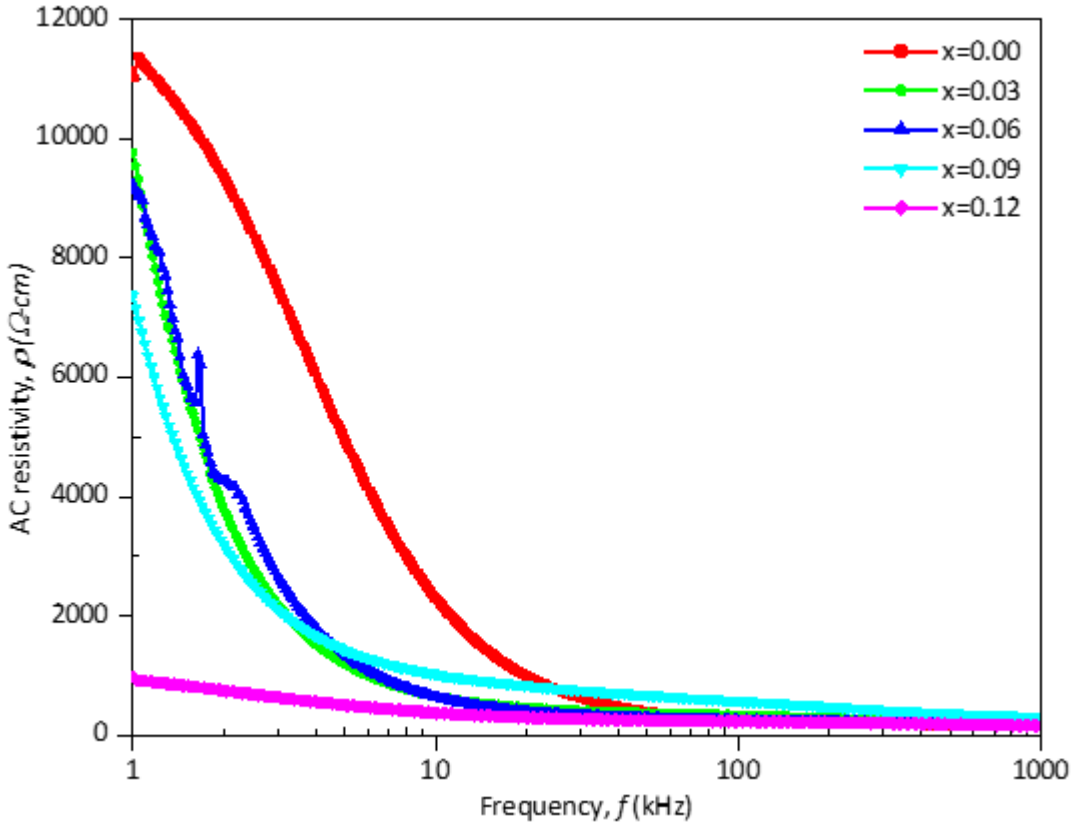

Fig. 9. The variation of AC resistivity with frequency of $Ni_{0.65}Zn_{0.35}Al_xFe_{2-x}O_4$(*x* = 0, 0.03, 0.06, 0.09, 0.12) ferrites.

Table 1. Structural data of Al-substituted Ni-Zn ferrites ($Ni_{0.65}Zn_{0.35}Al_xFe_{2-x}O_4$, where *x* = 0, 0.03, 0.06, 0.09, 0.12).

Al-content (*x*)	Molecular mass of the sample, *M* (gm)	Lattice constant, *a* (Å)	X- ray density, d_x (gm.cm^{-3})	Bulk density, d_B (gm.cm^{-3})	Porosity, *P* (%)
0.00	236.73	8.4052	5.31	4.96	6.21
0.03	236.58	8.3917	5.32	4.89	8.01
0.06	236.43	8.3881	5.34	4.86	8.69
0.09	236.33	8.3816	5.36	4.83	9.40
0.12	236.29	8.3715	5.37	4.79	10.52

Table 2. Elemental compositions of Al-substituted Ni-Zn ferrites ($Ni_{0.65}Zn_{0.35}Al_xFe_{2-x}O_4$**, where *x* = 0, 0.03, 0.06, 0.09, 0.12) determined *via* EDX studies.**

Al-content, *x*	Element % of Ni	Element % of Zn	Element % of Al	Element % of Fe	Element % of O
0.00	25.2	12.8	-	57.8	4.2
0.03	27.1	12.4	0.8	54.6	5.1
0.06	23.2	13.5	1.2	55.2	6.9
0.09	29.7	14.1	1.7	49.1	5.2
0.12	24.2	13.4	1.8	53.3	7.3

Table 3. FTIR data of Al-**substituted** Ni-Zn ferrites ($Ni_{0.65}Zn_{0.35}Al_xFe_{2-x}O_4$, where *x* = 0, 0.03, 0.06, 0.09, 0.12).

Al-content, *x*	ν_1 (cm^{-1})	ν_2 (cm^{-1})
0.00	400	591
0.03	401	590
0.06	401	590
0.09	402	592
0.12	405	594

Table 4. Curie temperature of Al-**substituted** Ni-Zn ferrites ($Ni_{0.65}Zn_{0.35}Al_xFe_{2-x}O_4$, where x = 0, 0.03, 0.06, 0.09, 0.12).

Al-content, x	Tc (°C)
0.00	393
0.03	385
0.06	383
0.09	380
0.12	370